Supporting Information

Cationic Radical Metal–Organic Framework Enabling Low Water Evaporation Enthalpy and High Photothermal Conversion Efficiency for Solar-Driven Water Purification

Zi-Yu Wang, [ab‡]Rui Wang, [a‡]Hannah M. Johnson, [c]Lei Cai, [a]An-An Zhang, [a]Qiang Zhang[*c] and Tian-Fu Liu[*a]

[a.]State Key Laboratory of Structural Chemistry, Fujian Institute of Research on the Structure of Matter, Chinese Academy of Sciences Fuzhou, Fujian 350108, China. E-mail: tfliu@fjirsm.ac.cn

[b.]College of Chemistry, Fuzhou University, Fuzhou, Fujian 350002, PR China.

[c.]Department of Chemistry, Washington State University, Pullman, WA 99163, United States. E-mail: q.zhang@wsu.edu

‡ These authors contributed equally to this work.

content

S1 Materials and instrumentation

Unless otherwise mentioned, all reagents and solvents were purchased from commercial sources including $NiCl_2 \cdot 6H_2O$, ethanol (EtOH), Acetonitrile (CH_3CN), N,N-dimethylformamide (DMF), Acetone, 4, 4'-Bipyridine, 2, 4-Dinitrochlorobenzene, 1H-Pyrazol-4-amine, They were used as received without further purification.

The PXRD patterns were recorded by Rigaku Smartlab with grazing-incidence X-ray diffraction (GIXRD) mode. ^{1}H-NMR spectra were recorded on Bruker AVANCE III 400MHz spectrometers spectrometer. Electron paramagnetic resonance (EPR) measurements were performed at X-band~9.8 (GHz) using a Bruker Bruker-BioSpin EPR spectrometer at room temperature. The contact angle between the absorber and water was calculated by means of a dynamic contact angle tester (Theta lite). Thermal Gravimetric Analysis (TGA) was performed on a Seiko S-II instrument where the dried crystalline samples were heated at a rate of 5°C/min up to 900°C and then cooled to room temperature under N_2 atmosphere. Differential scanning calorimetry (DSC) were tested on DSC2-01486: samples were heated from 30°C at a rate of 20°C/min up to 150°C and then cooled to 30°C at a rate of 10°C/min under N_2 atmosphere. Optical diffuse reflectance spectra were measured at room temperature using a PerkinElmer Lambda-900 UV-Vis-NIR diffusion reflectance spectroscopy (DRS) equipped with an integrating sphere. A BaSO4 plate was used as a reference for sample measurements. Infrared (IR) thermal images were recorded by HIKMICRO thermographic handheld professional camera. X-ray photoelectron spectroscopy (XPS) measurements were performed on a Thermo ESCALAB 250 spectrometer, using non-monochromatic Al Kα X-ray as the excitation source. The obtained data were analyzed by CaSa XPS software with choosing C 1s (284.8 eV) as the reference line to compensate for surface-charging effects. Inductively coupled plasma spectroscopy (ICP) was measured by HORIBA Jobin Yvon Ultima2.

S2 Experimental Procedures

Synthesis of BPZV

The ligand BPZV was prepared by a literature method with improvement, as shown in Scheme S1. Firstly, 2,4-Dinitrochlorobenzene (7.0 g, 35 mmol) and 4,4'-Bipyridine (1.6 g, 10 mmol) were dissolved and refluxed in CH_3CN (30 mL). The mixture is stirred together at 90°C for 72 h, then cooled to room temperature. The suspension was washed several times by centrifugation with CH_3CN and acetone, and dry at 80°C for 24 h, light yellow powder

(1,1‘-bis(2,4-dinitrophenyl)-[4,4’-bipyridine]-1,1‘-diium dichloride) (TNV) was obtained. Secondly, TNV (600 mg, 1.7 mmol) and 1H-Pyrazol-4-amine (178 mg, 3.2 mmol) were dissolved and refluxed in EtOH (200 mL). The mixture is stirred at 90℃ for 48h, then cooled to room temperature. The suspension was washed several times using centrifugation with EtOH and acetone, and dried at 80℃ for 24 h, dark green powder was obtained.

Synthesis of PFC-771

$NiCl_2 \cdot 6H_2O$ (20 mg) and BPZV (10 mg) in 4 mL of water was ultrasonicated for 5 minutes, followed by addition of 100 μL DMF. The obtained solution was ultrasonicated for additional 5 minutes and transferred to a 25 mL Teflon lined high-pressure reactor. Then, heated in an oven at 130℃ for 72 h. Finally, then cooled to room temperature. The obtained brown powder was washed several times by centrifugation with H_2O and Acetone at 11000 rpm and the precipitate was dried under 80℃.

Fabrication of PFC-771 film by EPD:

30 mg PFC-771 particles were dispersed in 70 mL DMF/acetone solution by ultrasound for 15 minutes. Then, two identical round-shaped Cu foam connecting with cathodic and anodic electrode with a separation distance of 2 cm were dipped into the above solution, and a dark deposition on negative electrode was distinguished after applying a direct current (DC) voltage of 120 V for 10min (denoted as PFC-771/Cu). Repeat the above process three times to achieve a uniformly distributed film with a thickness of approximately 400 μm.

Gas Sorption Measurements:

The as-synthesized samples were soaked in acetone for 2 days with the supernatant being replaced by fresh acetone about every 10 h during the process to exchange and remove nonvolatile solvates (DMF). After removal of acetone by centrifugation, the samples were activated under vacuum at room temperature for 6 h and then dried again by using the “degas” function of instruments at 120°C for 10 h prior to gas adsorption. N_2 isotherm measurements were performed at 77K to pressure of 1 bar.

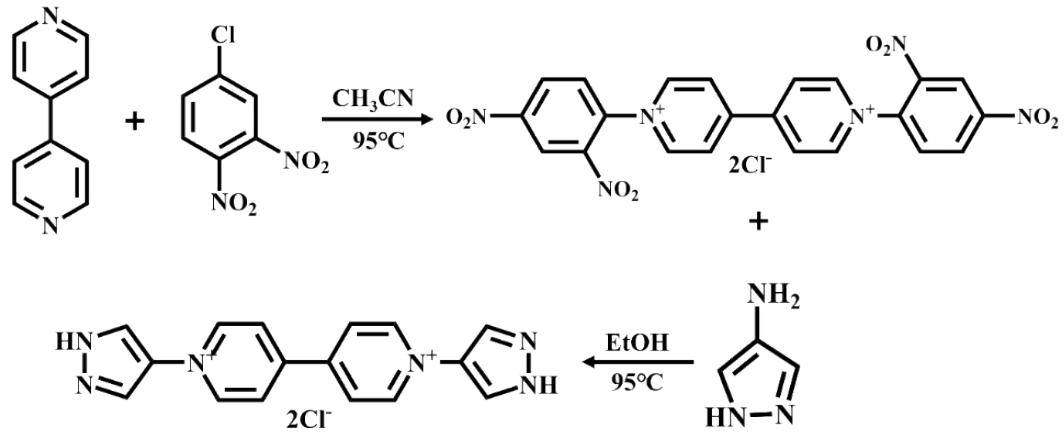

Scheme S1. Synthesis of BPZV ligand

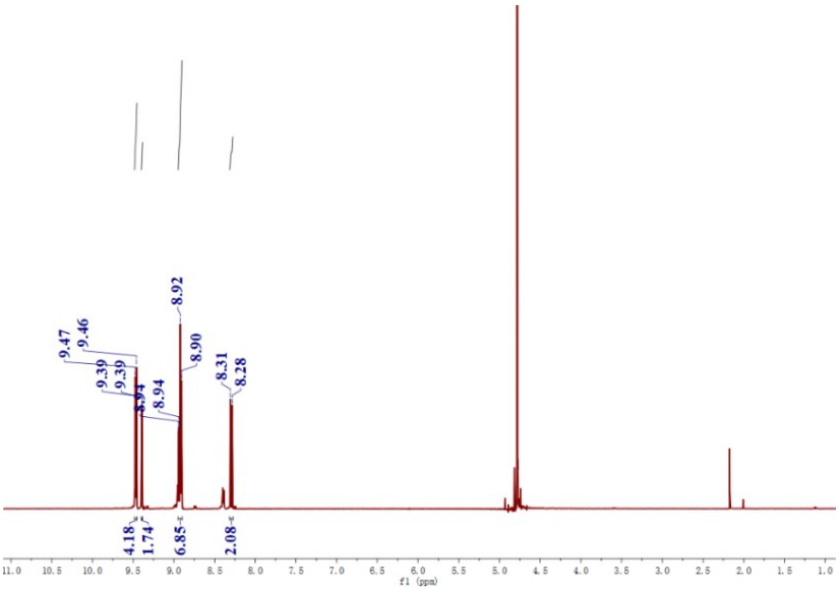

Figure S1. The ^{1}H NMR (400 MHz, D_2O) of TNV. ^{1}H NMR (400 MHz, D_2O): δ9.46~9.47 (d, 4H), 9.39 (d, 2H), 8.90~8.94 (m, 6H) and 8.28~8.31 ppm (d, 2H).

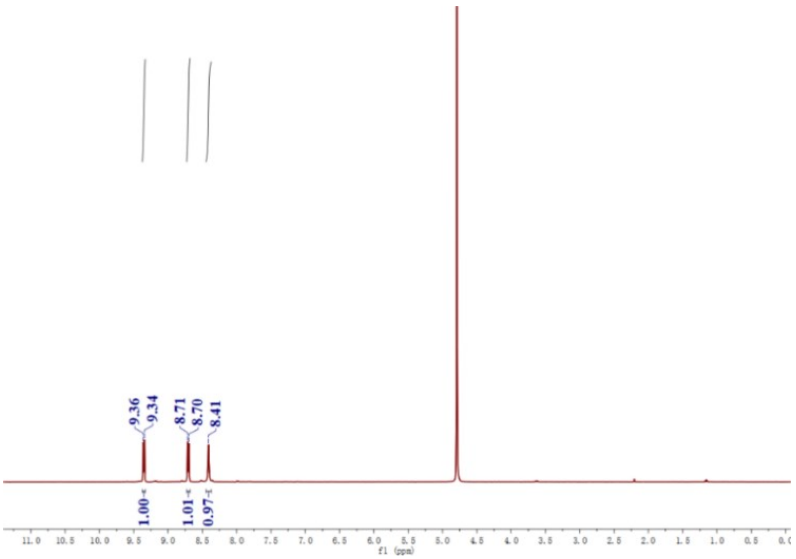

Figure S2. The ^{1}H NMR (400 MHz, D_2O) of BPZV. ^{1}H NMR (400 MHz, D_2O): δ9.34~9.36 (d, 4H), 8.70-8.71 (d, 4H) and 8.41ppm (s, 4H).

S3 Structural Characterizations of PFC-771

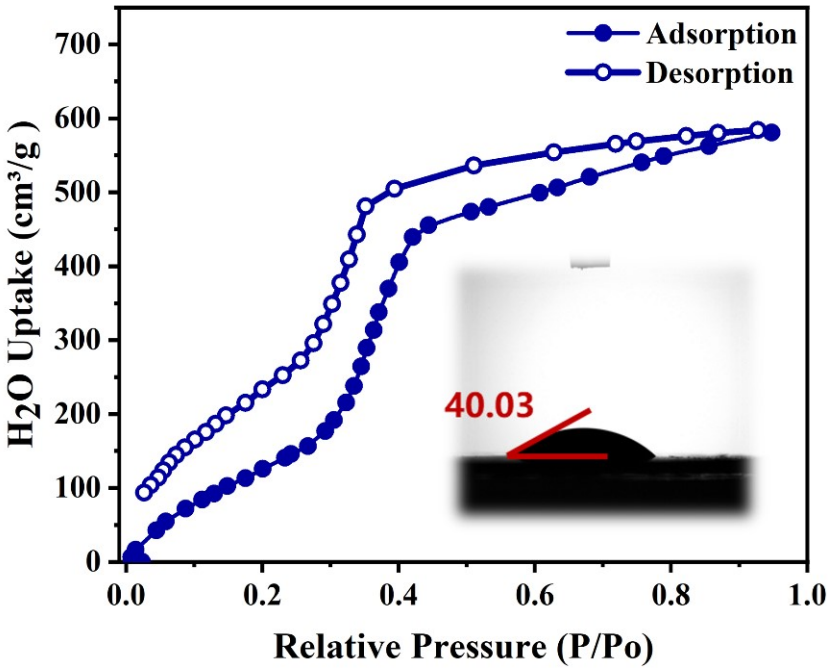

Figure S3. H_2O isotherm of PFC-771 at 298 K. (inset: Water contact angles of PFC-771)

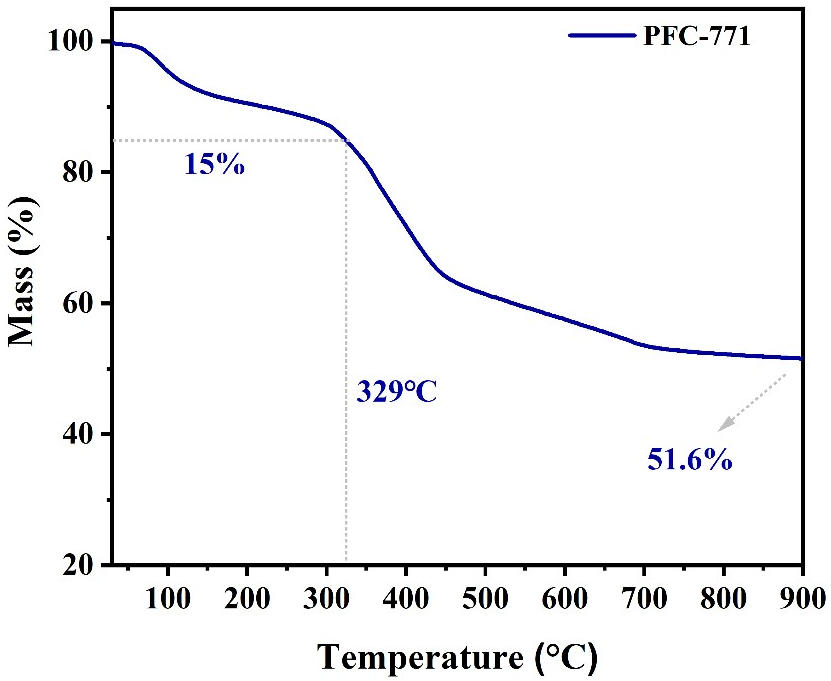

Figure S4. TGA curve of PFC-771.

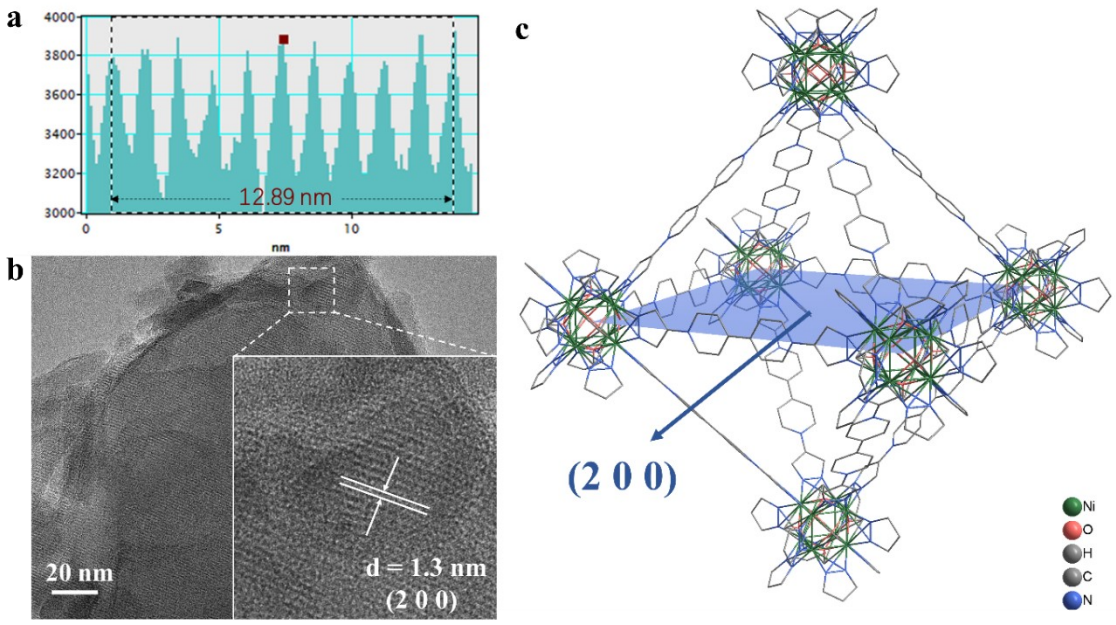

Figure S5. (a) FFT image of chosen area. (b) TEM images and the captured lattice fringes image of PFC-771. (c) The view of crystal structures showing the (200) plane of PFC-771.

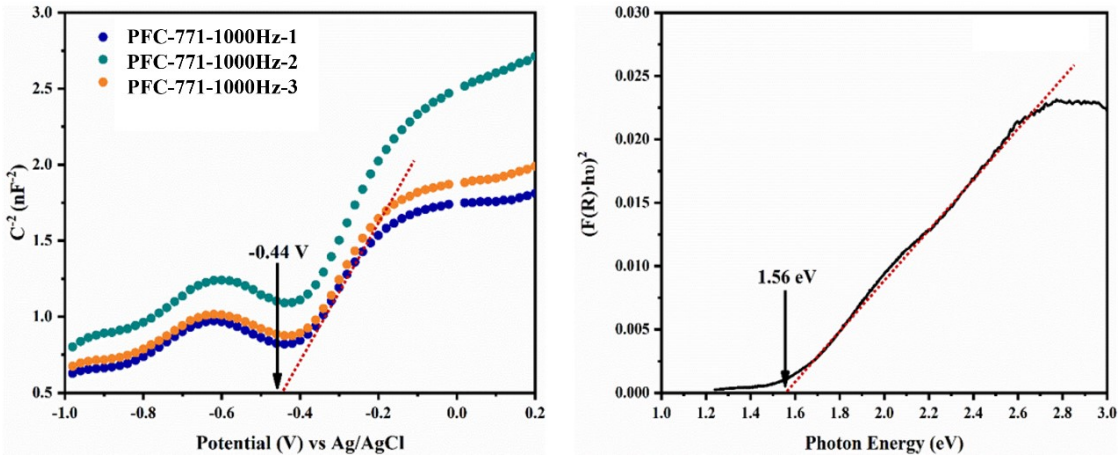

Figure S6. (a) Mott−Schottky plots for PFC-771 in 0.2 M Na_2SO_4 aqueous solution (b) DRS of PFC-771 and the band gaps deduced from K-M transformation.

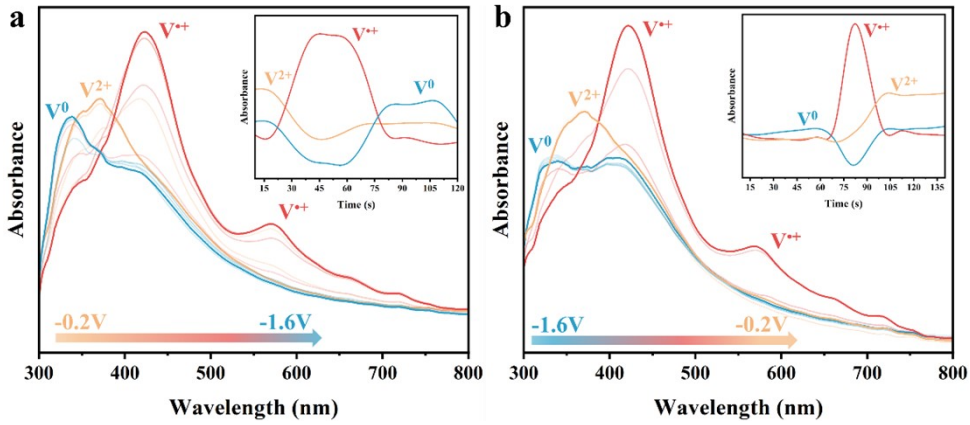

Figure S7. Spectroelectrochemical spectra of PFC-771 for electrochemical reduction (carried out from -0.2V to -1.6V) (a) and oxidation (carried out from -1.6V to -0.2V) (b) in 0.2 M Na_2SO_4 in intervals of 100 mV.

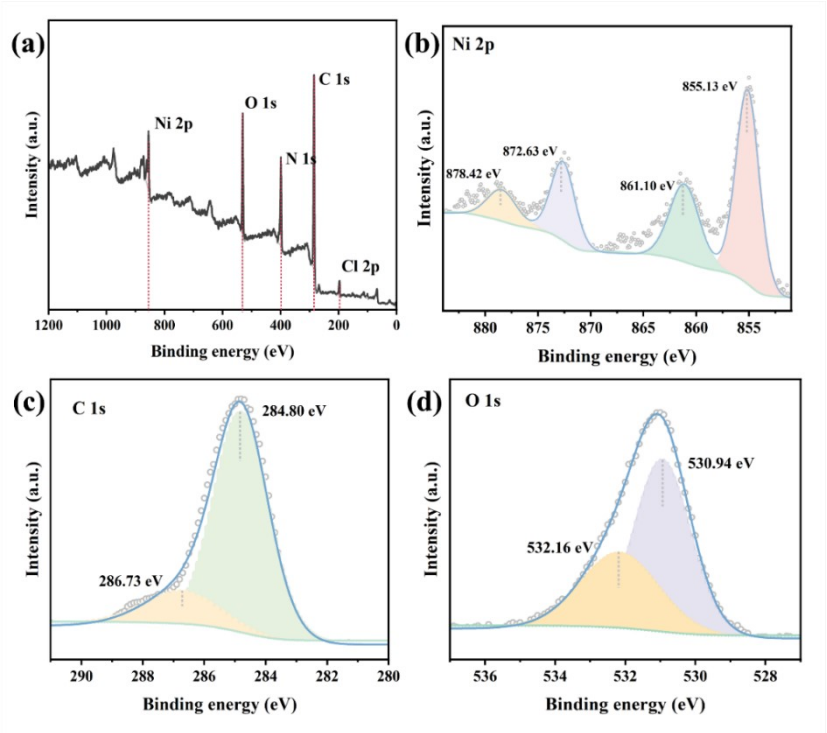

Figure S8. A full view of the XPS spectra (a) of PFC-771. (b) the close-ups for Ni 2p peaks. (c) C 1s peaks. and (d) O 1s peaks.

As shown in the XPS survey spectra of the sample, indicating the presence of Ni, O, C, N and Cl. The Ni 2p spectrum exhibits a characteristic doublet with energy peaks at 855.1 and 872.6 eV, corresponding to Ni $2p_{1/2}$ and Ni $2p_{3/2}$, respectively[1]. Figure S7c shows that the C 1s can be deconvolved into two different C environment corresponding to C-C (294.8 eV) and C=N (286.7 eV) bonds[2]. In the O 1s spectrum of the samples, O exists in the form H_2O (503.9 eV) and O-H (532.1 eV)[3].

S4 Structural Characterizations of PFC-771 film by EPD.

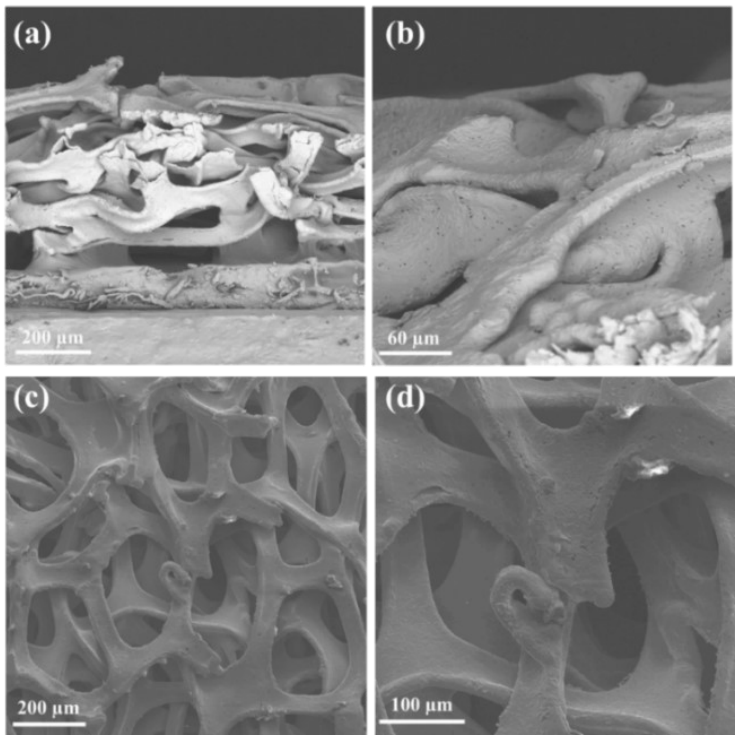

Figure S9. SEM images of bare Cu foam (a-b) cross-section SEM images (c-d) op-sectional SEM images.

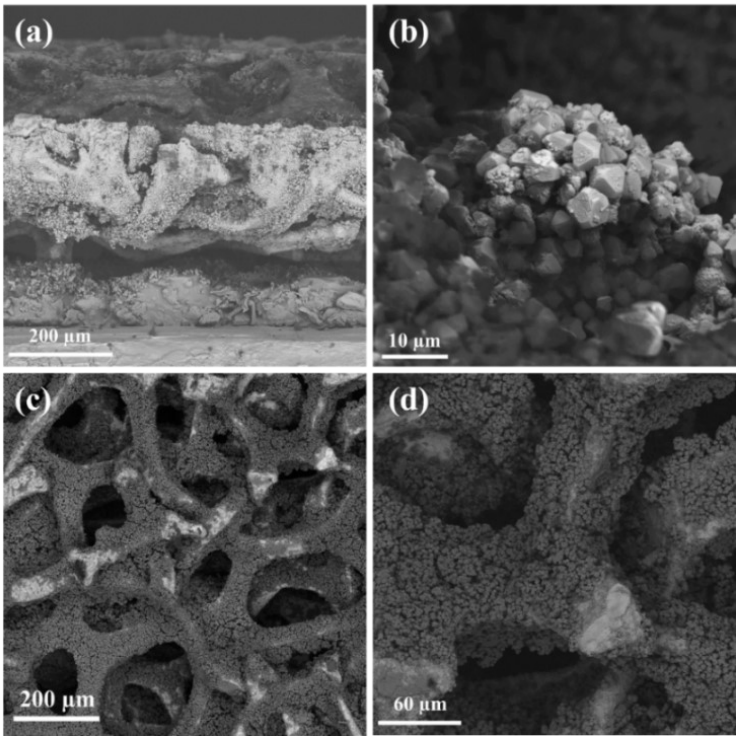

Figure S10. SEM images of PFC-771/Cu film (a-b) cross-section SEM images (c-d) top-sectional SEM images.

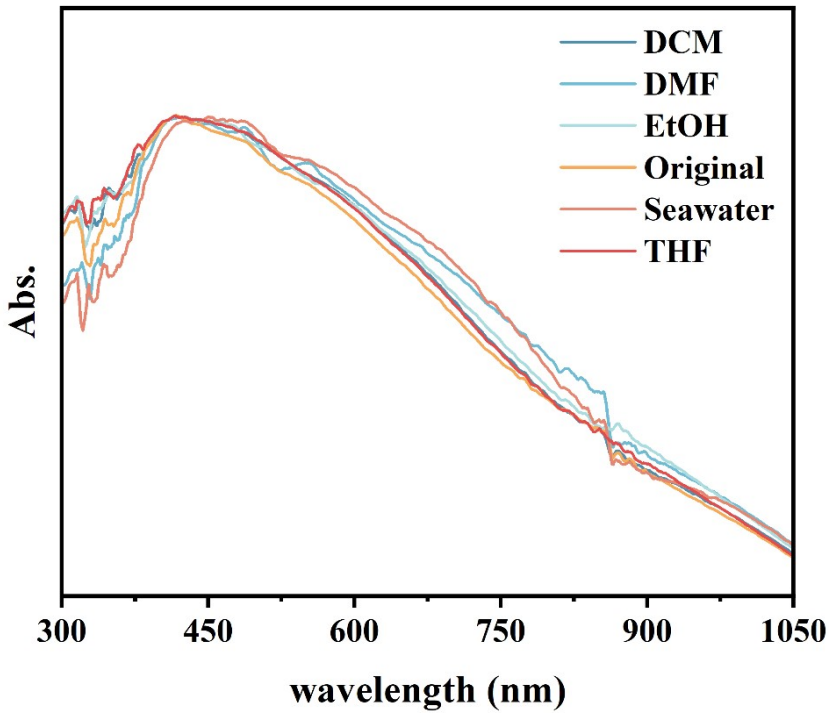

Figure S11. UV-Vis DRS of PFC-771 after immersing in different solvent for 24h.

S5 Photothermal Conversion Measurement.

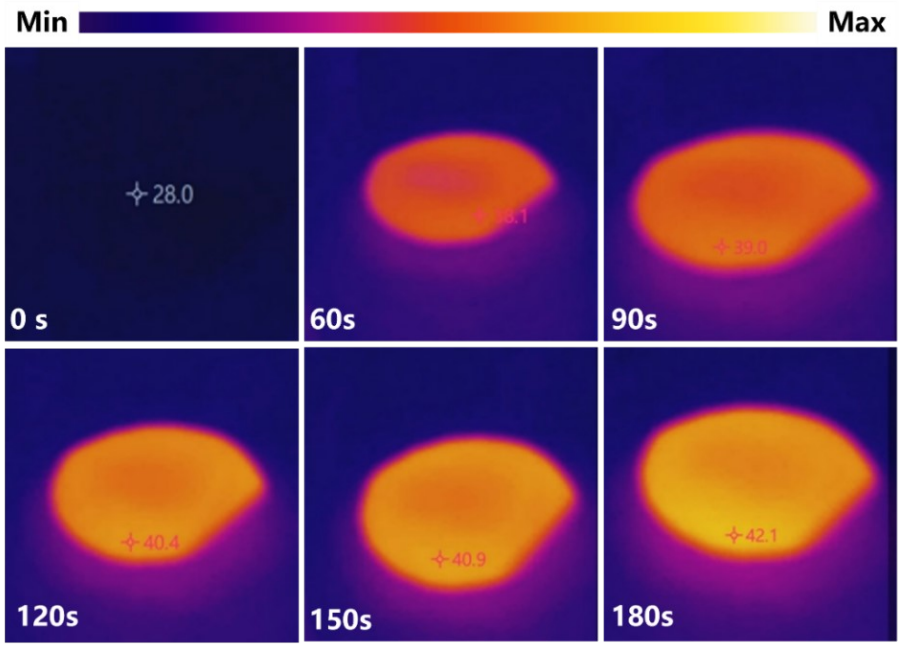

Figure S12. IR images of the PFC-771/Cu film (wet state) as a function of illumination time under one sun illumination.

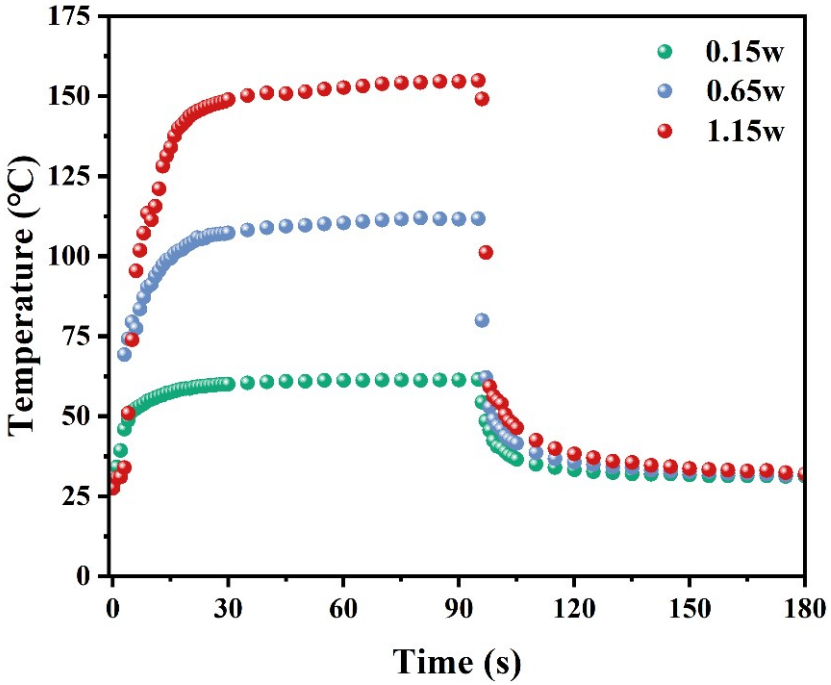

Figure S13. Photothermal conversion curves of PFC-771 on quartz glass under 980 nm laser irradiation with different intensities.

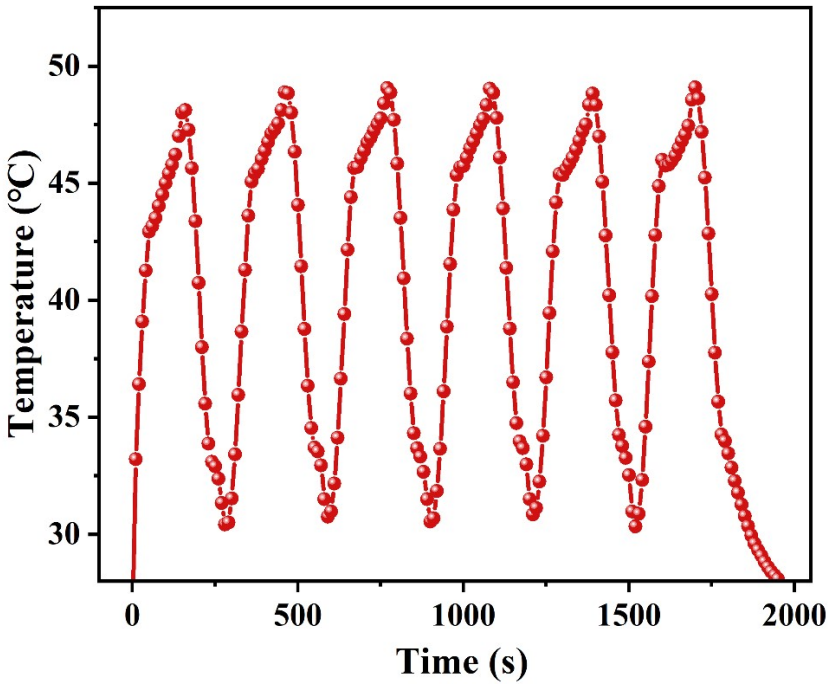

Figure S14. The heating and cooling curves of PFC-771 under on/off switch irradiation at 0.1 W·cm^{-2}.

S6 Solar-Driven Interfacial Water Evaporation.

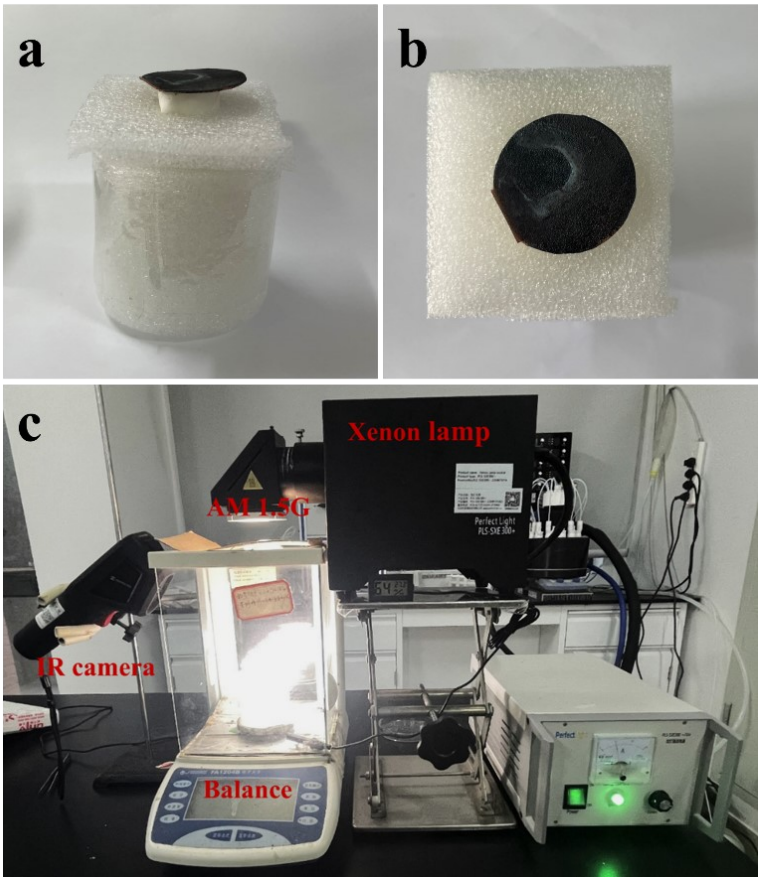

Figure S15. (a) The cross-sectional-view and (b) top-view photographs of the device, (c) Photograph for the device for recording the water mass change under solar irradiation. Under 1-sun (1 kW·m^{-2}) exposure in air, this simulation device was setup to monitor the changes in water weight over time.

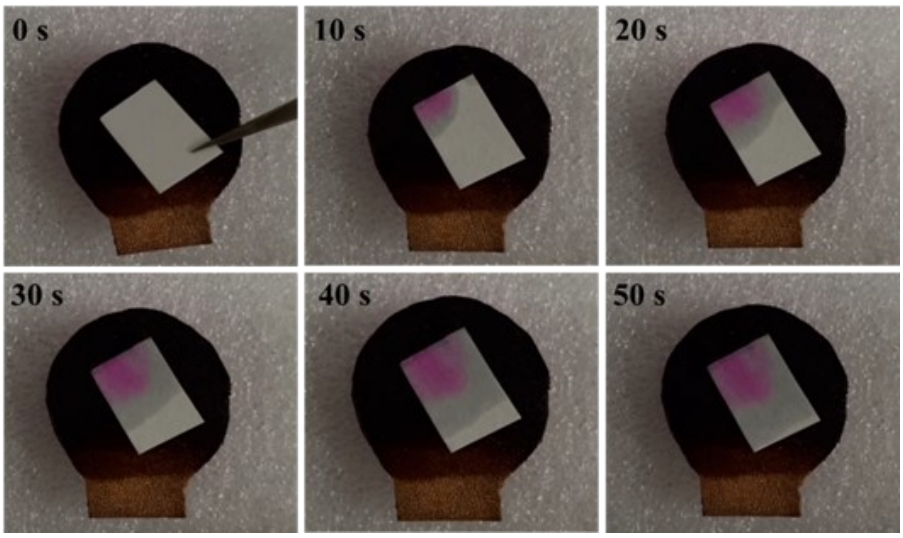

Figure S16. Dye solution absorption capacity of PFC-771/Cu film.

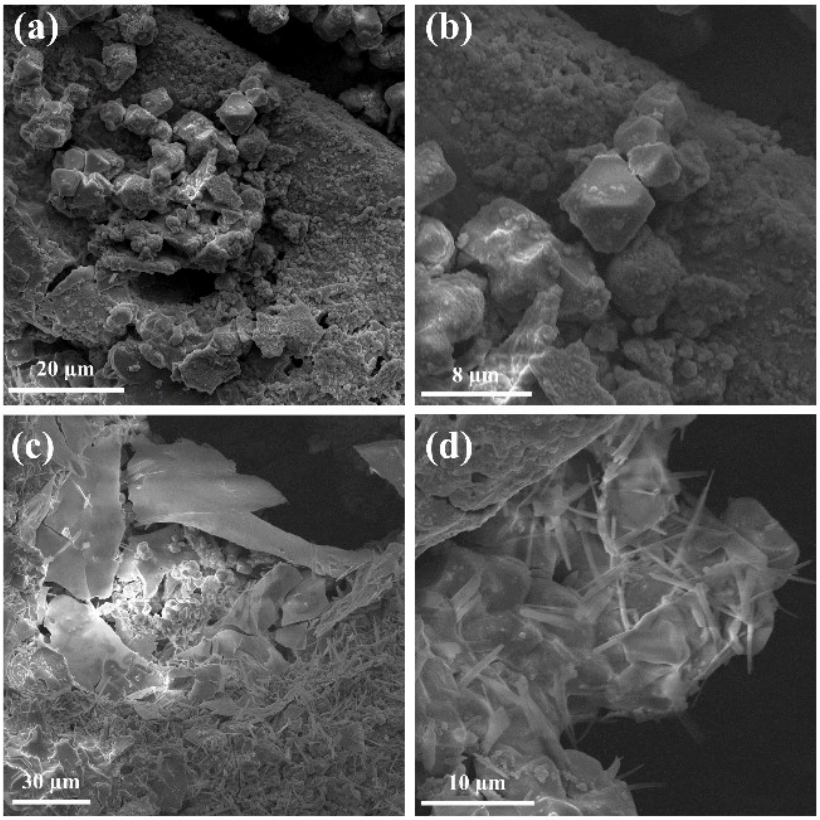

Figure S17. SEM images of PFC-771/Cu film after 14h evaporation.

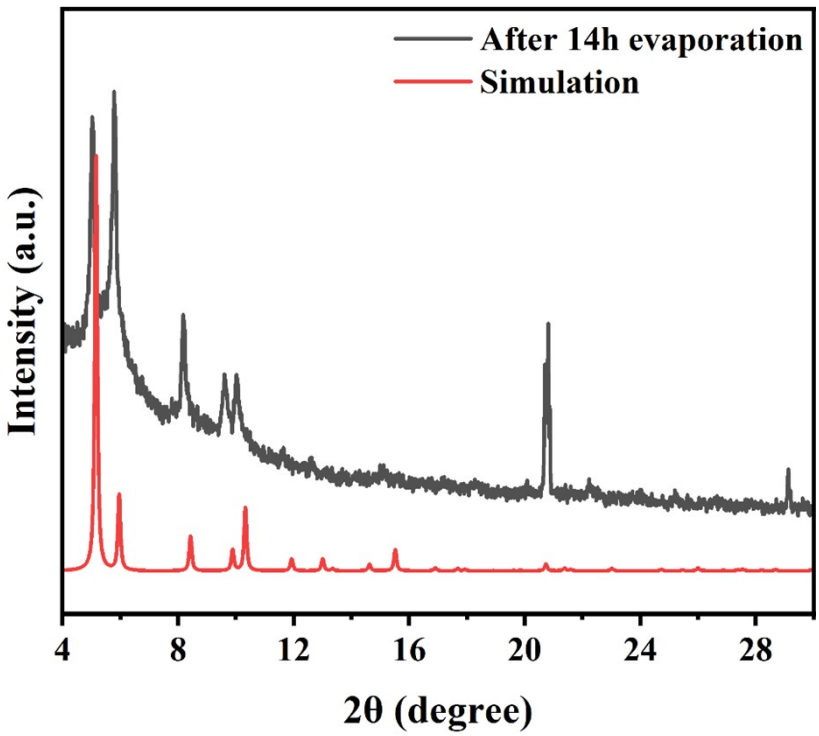

Figure S18. The PXRD pattern of PFC-771 after 14h evaporation.

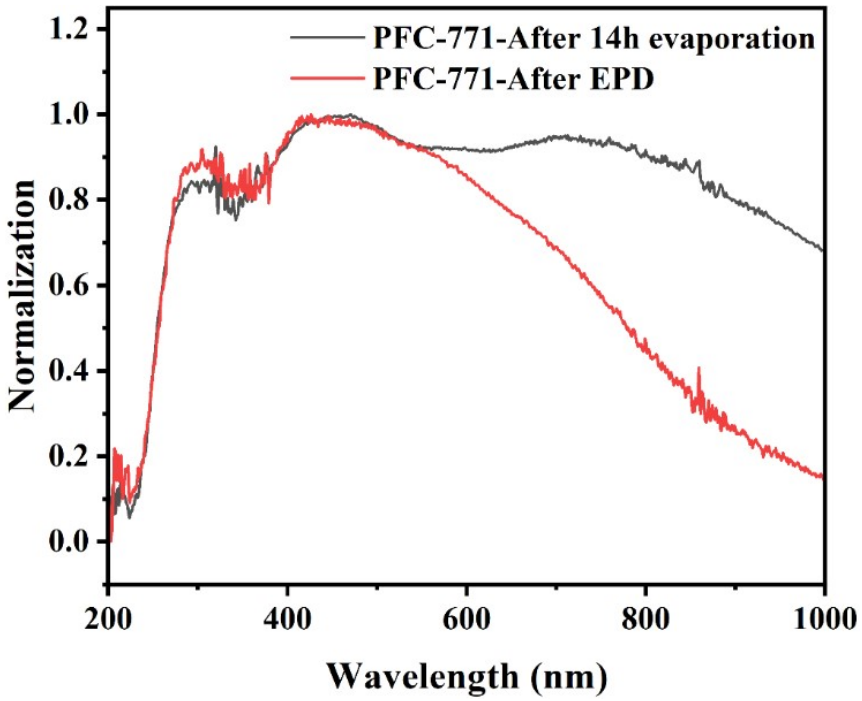

Figure S19. UV-Vis DRS of PFC-771 after 14h evaporation.

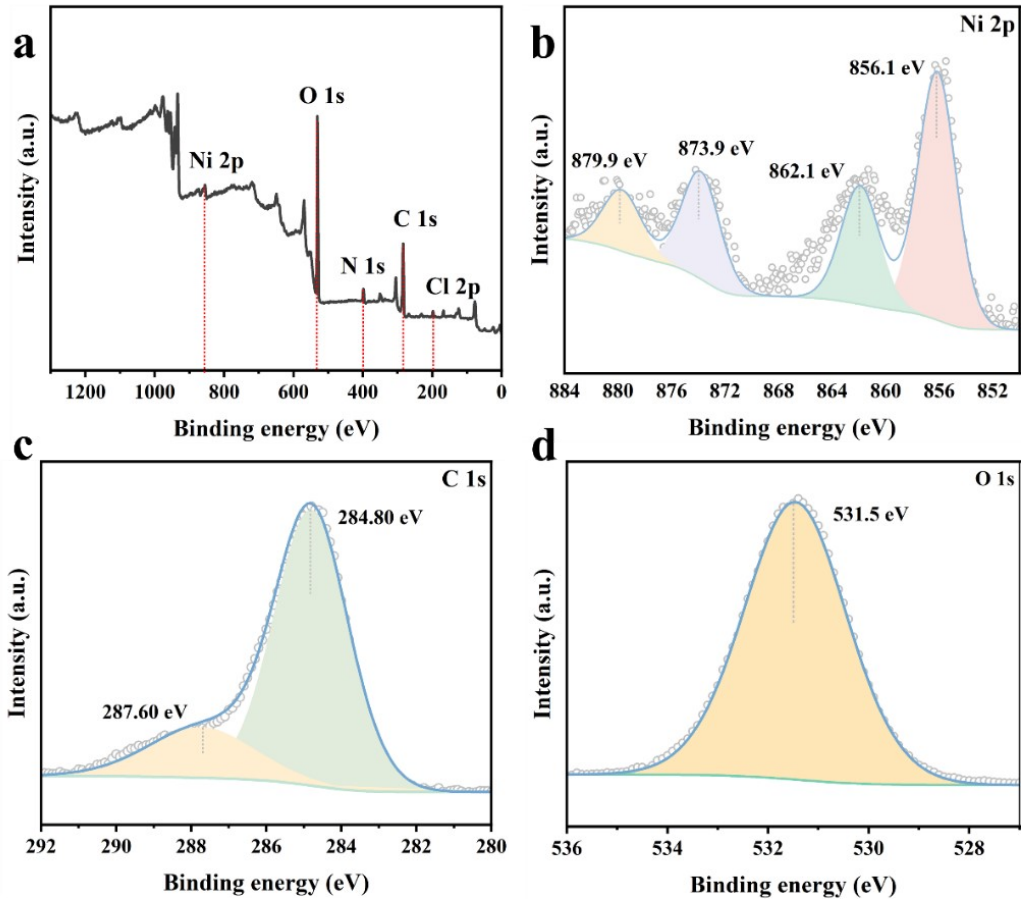

Figure S20. A full view of the XPS spectrum after 14h evaporation (a) of PFC-771. (b) the close-ups for Ni 2p peaks. (c) C 1s peaks and (d) O 1s peaks.

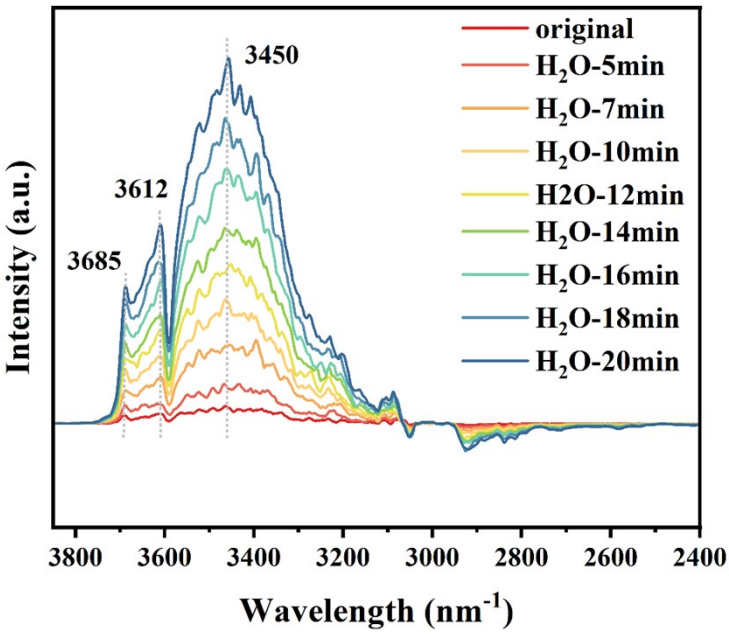

Figure S21. In situ FTIR spectra of H_2O absorbed in PFC-771 in the atmosphere of H_2O at 373K.

Table S1. Comparison of solar steam generation performance from literature reported polymers under one sun illumination.

Materials	**Evaporation rate ($kg \cdot m^{-2} \cdot h^{-1}$)**	**Efficiency (%)**	**Reference**
PFC-771/Cu foam	**1.33**	**91.08**	**This work**
Ppy/Alg hydrogel	1.15	54.1	Desalination 500 (2021) 114900[4]
CG@MPT-h sponges	1.13	78.9	ACS Appl. Mater. Interfaces 2021, 13, 10902−10915[5]
CR-TPE-T	1.272	87.2	Adv. Mater. 2020, 1908537[6]
GT-COF-3-loaded foam	1.314	90.7	CCS Chem. 2021, 3, 2926[7]
Polymer foam	1.17	80.5	Chem. Sci., 2018, 9, 623[8]
CNT@PEI/MCE	5.07	72.0	J. Mater. Chem. A, 2019, 7, 704–710[9]
MDPC/SS mesh	1.222	84.3	Sol. Energy Mater Sol. Cells. 2019, 196, 36–42[10]

S7 Calculation.

Supplementary Note 1: Calculation of the efficiency for solar vapor generation

The thermal efficiency (η) is considered to assess the performance of PFC-771/Cu film and is defined as[11]

$$\eta = \frac{\dot{m} h_{LV}}{C_{opt} P_0} \quad \text{(S5)}$$

where ṁ denotes the mass flux, C_{opt} the optical concentration and P_0 the nominal direct solar irradiation 1 kW·m^2, h_{LV} refers to total enthalpy of liquid–vapour phase change [i.e., sensible heat and vaporization enthalpy (h_{LV} = Q + Δh_{vap})]. The schematic diagram of the vaporization enthalpy of steam is as follows:

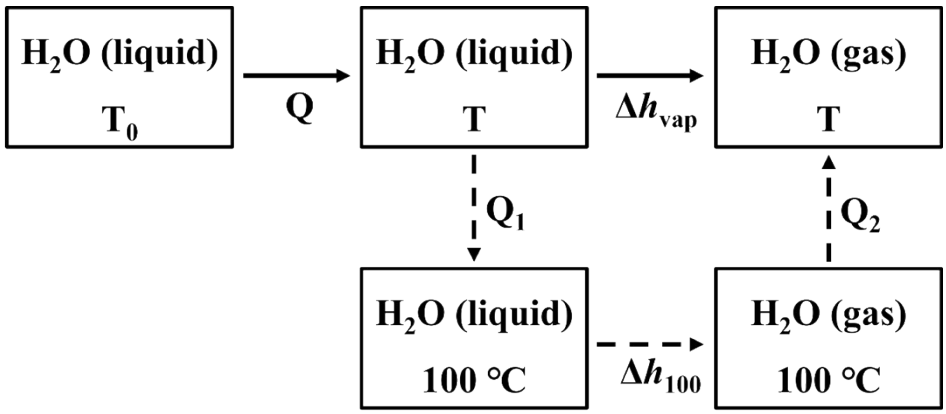

$$Q = C_{liquid} \times (T - T_0) \quad \text{(S6)}$$

$$\Delta h_{vap} = Q_1 + \Delta h_{100} + Q_2 \quad \text{(S7)}$$

$$Q_1 = C_{liquid} \times (100 - T) \quad \text{(S8)}$$

$$Q_2 = C_{gas} \times (T - 100) \quad \text{(S9)}$$

In this work, C_{liquid}, the specific heat capacity of liquid water is a constant of 4.18 J·g^{-1}·°C^{-1}. C_{gas}, the specific heat capacity of water vaper is a constant of 1.865 J·g^{-1}·°C^{-1}. Δh_{100} is the latent heat of vaporization of water at 100°C, taken to be 2260 kJ·kg^{-1}

For example, the surface temperature of PFC-771/Cu film was 42.1°C during the evaporation process, therefore T is 37.6°C. According to the above formula,

Q = 4.18 × (42.1- 25) = 71.478 kJ·kg^{-1}

Δh_{100}= 4.18×(100 – 42.1)+2260+1.865× (42.1 - 100) = 2394.039 kJ·kg^{-1}

h_{LV} = Q + Δh_{vap} = 71.478 + 2394.039 = 2465.517 kJ·kg^{-1}

ṁ = 1.33 kg·m^{-2}·h^{-1}

P_0 = 1 kW·m^{-2}

C_{opt} = 1

$$\eta = \frac{\dot{m}h_{LV}}{C_{optP0}} = \frac{1.33 \times 2465.517}{3600} \times 100\% = 91.08\%$$

As a result, evaporation efficiency η = 91.08% when the latent heat of water vaporization at 42.1°C is used in calculation.

Table S2 The evaporation rate and efficiency corresponding to different amounts of PFC-771.

m/m_0	T (K)	T_0 (K)	h_{LV} (kJ·kg^{-1})	$\dot{m}$ (kg·m^{-2}·h^{-1})	η (%)
2.92%	308	303	2430.63	0.925	62.48
3.73%	309	303	2431.75	1.094	73.89
4.46%	311	306	2436.97	1.185	79.80

Table S3 Evaporation rate and efficiency

Evaporator	T (K)	T_0 (K)	h_{LV} (kJ·kg^{-1})	$\dot{m}$ (kg·m^{-2}·h^{-1})	η (%)
PFC-771/Cu	310.6	298	2465.51	1.333	91.08
Cu foam	299	290	2456.39	0.298	20.34
Bulk water	301	290	2437.36	0.356	24.29

Supplementary Note 2: Calculation of heat loss[12]

The calculation process for the light intensity of 1 kW·m^{-2} is shown as an example. The solar energy absorbed by a PFC-771/Cu film solar evaporator (Q_{in}) can be calculated by

$$Q_{in} = S \times q_i \times t \quad \text{(S11)}$$

where S is the projection area of the evaporator (d=1.5 cm), q_i is the light intensity and t is the time of illumination.

The heat loss (η_{hl}) mainly consists of radiation loss, convection loss and conduction loss.

1. Radiation loss

The radiation loss (η_{rad}) can be calculated by

$$\eta_{rad} = \frac{S\varepsilon\sigma(T_1^4 - T_0^4)}{S \times q_i} = \frac{\varepsilon\sigma(T_1^4 - T_0^4)}{q_i} \quad \text{(S12)}$$

where S is the projected area of the evaporator (d=1.5 cm), ε is the emissivity (about 0.84), σ is the Boltzmann constant (5.67 × 10-8 $W \cdot m^{-2} \cdot K^{-4}$), T_1 is the temperature of the evaporator surface, and T_0 is the ambient temperature. In our work, at a light intensity of 1 kW m^{-2}, T_1=315.1 K and T_0 = 298 K, so η_{rad}=9.3%

2. Convection loss

The convection loss (η_{conv}) can be calculated according to

$$\eta_{conv} = \frac{Sh(T_1 - T_0)}{S \times q_i} = \frac{h(T_1 - T_0)}{q_i} \quad \text{(S13)}$$

where S is the projected area of the evaporator (d=1.5 cm), h is the convective heat transfer coefficient (5 $W \cdot m^{-2} \cdot K^{-1}$), T_1 is the surface temperature of the evaporator, and T_0 is the ambient temperature. In our work, at a light intensity of 1 $kW \cdot m^{-2}$, T_1 = 313.45 K and T_0 = 298.65 K, so η_{conv}= 8.5%.

3. Conduction loss

We employ a 1D water transport pathway to isolate the solar absorber from with the water, so the conduction loss can be ignored.

In summary, at a light intensity of 1 $kW \cdot m^{-2}$, the total heat loss η_{hl}=17.8%.

Supplementary Note 3: Calculation of the water evaporation enthalpy

The energy for water evaporation in dark is obtained from the environment, which is thereby same for different evaporators, according to the previous work[13]. Considering the known theoretical evaporation enthalpy value of liquid water (ca. 2430 $kJ \cdot kg^{-1}$), the water evaporation enthalpy values of the PCF-771/Cu film evaporator are calculated by the following formula,

$$U_{in} = E_{equ}M_g = E_0M_0 \quad \text{(S10)}$$

where U_{in} is the total energy absorbed from the environment per hour; E_0 refers to the water evaporation enthalpy (2430 $kJ \cdot kg^{-1}$), M_0 refers to the water mass loss (g) in 1 h of evaporation system without evaporators in the darkness, respectively; M_g means the water mass loss (g) of evaporation system with the evaporator; E_{equ} is the equivalent evaporation enthalpy of the corresponding system.

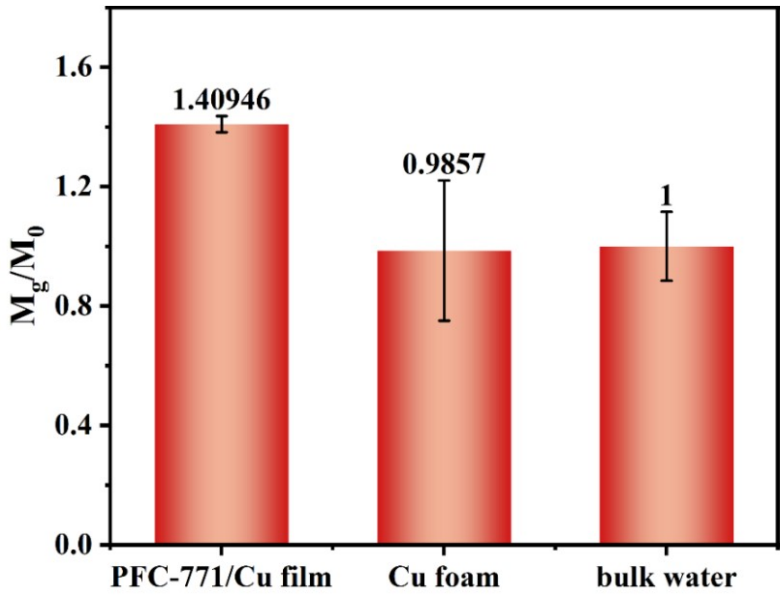

Figure S22. The ratio between M_g and M_0.

In the darkness, the M_g/M_0 loss of bulk water, bare Cu foam, and PFC-771/Cu film is 1, 0.98, and 1.41, respectively. Hence, the water evaporation enthalpy of the bare Cu foam and PFC-771/Cu film is calculated to be 2465 kJ·kg^{-1} and 1724 kJ·kg^{-1}, respectively, which is lower than that of the bulk water (2430 kJ·kg^{-1}). The evaporation enthalpy estimated by the evaporation process in a dark environment (1724 kJ·kg^{-1}) shows the similar trend, but lower than that obtained through the DSC method (2184.37 kJ·kg^{-1}). The reason can be attributed to the fact that DSC measures the process of completely dehydration, whereas actual solar water evaporation involves partial dehydration.

Table S4. Comparison of energy consumption estimated from DSC measurement and dark experiment.

Energy consumption(kJ·kg^{-1})	**PFC-771/Cu**	**Cu foam**	**Bulk water**
DSC measurement	2184.37	2294.19	2206. 60
Dark experiment	1724	2465	2430

References：

1. S. N. Sun, L. Z. Dong, J. R. Li, J. W. Shi, J. Liu, Y. R. Wang, Q. Huang and Y. Q. Lan, Angew. Chem. Int. Ed. 2022, **61**,e202207282.
2. Q. Chen, S. Li, H. Xu, G. Wang, Y. Qu, P. Zhu and D. Wang, , Chinese J. Catal, 2020. **41**, 514-523.
3. M. Zheng, Y. Ding, L. Yu, X. Du and Y. Zhao, Adv. Funct. Mater, 2017, **27**, 1605846.
4. S. H. Park, J. H. Park, J. Kim and S. J. Lee, Desalination, 2021, **500**, 114900.
5. X. Wang, Z. Li, Y. Wu, H. Guo, X. Zhang, Y. Yang, H. Mu and J. Duan, Appl. Mater. Interfaces 2021, **13**, 10902−10915.
6. G. Chen, J. Sun, Q. Peng, Q. Sun, G. Wang, Y. Cai, X. Gu, Z. Shuai and B. Z. Tang, Adv. Mater. 2020, 1908537.
7. X. Tang, Z. Chen, Q. Xu, Y. Su, H. Xu, S. Horike, H. Zhang, Y. Li and C. Gu, CCS Chem. 2021, **3**, 2926.
8. Q. Chen, Z. Pei, Y. Xu, Z. Li, Y. Yang, Y. Wei and Y. Ji, Chem. Sci., 2018, **9**, 6238.
9. Y. Li, X. Cui, M. Zhao, Y. Xu, L. Chen, Z. Cao, S. Yang and Y. Wang, J. Mater. Chem. A, 2019, **7**, 704–7109.
10. S. Ma, W. Qarony, M. I. Hossain, C. T. Yip and Y. H. Tsang, Sol. Energy Mater Sol. Cells. 2019, **196**, 36–4210.
11. X. Ye, L.-H. Chung, K. Li, S. Zheng, Y.-L. Wong, Z. Feng, Y. He, D. Chu, Z. Xu, L. Yu and J. He, Nat. Commun, 2022, **13**, 1-8.
12. Q. Yongqiang, X. Guanfeng, C. Luzhuo, X. Gang and E. W. Guan, Adv. Mater, 2023, **36**, 2310795.
13. X. Zhou, Y. Guo, F. Zhao, W. Shi and G. Yu, Adv. Mater, 2020, **32**, 2007012.